The Role of Acantharia in Southern Ocean Strontium Cycling and Carbon Export: Insights from Dissolved Strontium Concentrations and Seasonal Flux Patterns

Yaojia Sun[1], Cathryn Wynn-Edwards[2], Thomas W. Trull[2], and Michael J Ellwood[1]

[1]Australian National University
[2]CSIRO

March 07, 2024

Abstract

Dissolved strontium (Sr) concentrations in the Southern Ocean water samples and Sr export fluxes from sediment trap moorings at 1000 m were used to assess particulate organic carbon (POC) export associated with Acantharia for 2010, 2018 and 2020. The dissolved Sr data revealed a prominent vertical gradient with lower surface Sr concentrations depleted up to 1.4% relative to deep waters. A strong latitudinal surface gradient was observed, ranging from 87.3 near the northern end to 88.5 near the southern end of a transect through the Australian sector of the Southern Ocean. These findings highlight the significant role that Acantharia, which precipitate celestite (SrSO4), play in marine Sr cycling. Seasonal variability in Sr export fluxes can be large, particularly during intense events in summer, and reaches a maximum of 2.8 , contributing up to 7% of the POC export flux. The coincidence of Sr flux with the second peak of POC export flux implies a potential association of Acantharia biomass with summertime productivity.

Hosted file

983852_0_art_file_11745477_s6rh30.docx available at https://authorea.com/users/714342/articles/698612-the-role-of-acantharia-in-southern-ocean-strontium-cycling-and-carbon-export-insights-from-dissolved-strontium-concentrations-and-seasonal-flux-patterns

Hosted file

983852_0_supp_11745478_s6rh30.docx available at https://authorea.com/users/714342/articles/698612-the-role-of-acantharia-in-southern-ocean-strontium-cycling-and-carbon-export-insights-from-dissolved-strontium-concentrations-and-seasonal-flux-patterns

The Role of Acantharia in Southern Ocean Strontium Cycling and Carbon Export: Insights from Dissolved Strontium Concentrations and Seasonal Flux Patterns

Yaojia Sun[1], Cathryn A. Wynn-Edwards[2,3], Thomas W. Trull[2,3], Michael J. Ellwood[1,4]

[1]Research School of Earth Sciences, Australian National University, Canberra, ACT, Australia.

[2]Australian Antarctic Program Partnership, Institute for Marine and Antarctic Studies, University of Tasmania, Hobart, TAS, Australia.

[3]Oceans and Atmosphere, Commonwealth Scientific and Industrial Research Organisation, Hobart, TAS, Australia.

[4]Australian Centre for Excellence in Antarctic Science (ACEAS), Australian National University, Canberra, ACT, Australia.

Corresponding author: Yaojia Sun (yaojia.sun@anu.edu.au)

Key Points:

- Strong vertical and latitudinal gradient of dissolved Sr observed in the Southern Ocean driven by Acantharia
- Sr export fluxes exhibit seasonal variations with peaks occur annually in summer, contributing up to 7% to POC flux
- Elevated Acantharia biomass is possibly associated with summertime productivity

Abstract

Dissolved strontium (Sr) concentrations in the Southern Ocean water samples and Sr export fluxes from sediment trap moorings at 1000 m were used to assess particulate organic carbon (POC) export associated with Acantharia for 2010, 2018 and 2020. The dissolved Sr data revealed a prominent vertical gradient with lower surface Sr concentrations depleted up to 1.4% relative to deep waters. A strong latitudinal surface gradient was observed, ranging from 87.3 $\mu mol\ kg^{-1}$ near the northern end to 88.5 $\mu mol\ kg^{-1}$ near the southern end of a transect through the Australian sector of the Southern Ocean. These findings highlight the significant role that Acantharia, which precipitate celestite ($SrSO_4$), play in marine Sr cycling. Seasonal variability in Sr export fluxes can be large, particularly during intense events in summer, and reaches a maximum of 2.8 $mg\ Sr\ m^{-2}d^{-1}$, contributing up to 7% of the POC export flux. The coincidence of Sr flux with the second peak of POC export flux implies a potential association of Acantharia biomass with summertime productivity.

Plain Language Summary

Acantharia are tiny marine organisms found worldwide. Their skeletons and cysts, composed of a heavy mineral called strontium sulfate ($SrSO_4$, also called celestite), make them important in the ocean's strontium cycling. Despite having skeletons and cysts dense enough to potentially act as effective ballast, Acantharia were previously not believed to substantially impact carbon export in the deeper ocean layers due to their high solubility in seawater. Our study focused on understanding how Acantharia influence strontium cycling and contribute to carbon export in the Southern Ocean. We discovered that Acantharia efficiently remove strontium from the ocean's surface and release it at intermediate depths. These organisms exhibit seasonal variations and are particularly abundant in summer, contributing up to 7% to particulate organic carbon export during the summer productive season. This is significant for the Southern Ocean as a major region for carbon sequestration and global climate buffering.

1. Introduction

Marine protists, particularly Acantharia, play a significant role in the biogeochemical cycles of carbon (C) and strontium (Sr) in the ocean. Acantharia are characterized by an internal star-

shaped skeleton made of celestite, a strontium sulphate ($SrSO_4$) mineral (Decelle and Not, 2015). These organisms are the only known marine species that precipitate celestite from the dissolved form, making them potentially important in oceanic Sr cycling (de Villiers, 1999). Phylogenetic analyses have identified nine molecular clades of Acantharia, with early diverging clades A, B and C forming cysts for reproduction (Decelle and Not, 2015). Acantharian cysts, composed of high-density celestite (3.96 g m-3), can grow up to 1-2 mm, usually exceeding the size of adult Acantharian cells (Martin et al., 2010; Decelle and Not, 2015; Mars Brisbin et al., 2020). The high density of Acantharian cysts results in high sinking rates (up to 770 m d^{-1}) (Martin et al., 2010), allowing them to sink to bathypelagic depths (1500 – 2000 m) before dissolving (Martin et al., 2010; Belcher et al., 2018). Once the cyst is formed, the enclosed cytoplasm transforms into numerous flagellated swarmers of less than 5 µm in size, which are eventually released through pores in the cysts or when the cyst walls rupture (Schewiakoff, 1926; Spindler and Beyer, 1990). The most recently diverged clades E and F do not form cysts. Instead, clades E and F host intracellular symbiotic microalgae from the haptophyte genus *Phaeocystis* (Decelle et al., 2012). This symbiotic relationship is beneficial for Acantharia, as it enhances their nutrient acquisition by fixing organic carbon through photosynthesis and improves their efficiency in using prey biomass with the energy substrate provided by the symbionts (Michaels, 1988, 1991; Michaels et al., 1995). Symbiotic Acantharia are important for primary production, especially in low-chlorophyll conditions where they can contribute up to 20% of the total primary production (Michaels, 1988, 1991; Caron et al., 1995).

The Southern Ocean is characterized by high-nutrient, low-chlorophyll (HNLC) conditions with particulate organic carbon (POC) export fluxes in the subantarctic region ranging from 1 to 1.4 $\mathrm{g\,C\,m^{-2}yr^{-1}}$, which is close to the global median (Trull et al., 2001; Cathryn A. Wynn-Edwards et al., 2020a). Previous studies have identified calcium carbonate ($CaCO_3$) from calcifying organisms and opal from diatoms as dominant ballasting minerals in this region (Cathryn A. Wynn-Edwards et al., 2020a). However, Acantharia, which dominate protozooplankton assemblages in the Southern Ocean and have the potential for significant ballasting of POC (Henjes et al., 2007; Assmy et al., 2014), have been overlooked due to their high solubility as seawater is undersaturated with respect to $SrSO_4$ (North, 1974; Reardon and Armstrong, 1987). Recent studies have shown that Acantharia can contribute significantly to POC flux to the

bathypelagic zone in high-latitude regions where they may be less prone to dissolution (Belcher et al., 2018). In the Iceland Basin, Martin et al. (2010) observed that Acantharia contribute 48% to the POC flux at 2000 m during a two-week sampling interval, but their contribution to the annual POC flux did not exceed 1-2%, likely because Acantharian fluxes vary seasonally. Recently, Belcher et al. (2018) reported high Acantharian fluxes of 5.1 $\mathrm{mg\,C\,m^{-2}d^{-1}}$ at 1500 m in the Scotia Sea, accounting for 26% of POC flux during the productive season and 17% of the annual POC flux in this region.

Despite their potential contribution to annual sedimentation in high latitude oceans, the mechanisms driving Acantharia fluxes are poorly understood. One hypothesis is that in high latitudes where seasonality is most pronounced, Acantharia tend to release swarmers at depth to avoid predation. This strategy allows swarmers and juveniles to access the pulse of organic matter following a phytoplankton bloom as they ascend toward the surface. In contrast, Acantharia in low latitudes tend to form swarmers at the upper mesopelagic layer, possibly due to a greater supply of fresher organic matter in the upper mesopelagic compared to deep waters, potentially fewer predators, and more constant particle flux due to weaker seasonality (Martin et al., 2010; Decelle et al., 2013).

In this study, we explore the relationship between Acantharia, dissolved and particulate Sr concentrations, and carbon export to provide a better understanding of the role of Acantharia in Sr and C cycles as well as their life strategies and cycles. This is particularly important for the Southern Ocean, which is a major region for carbon sequestration and plays a vital role in regulating the oceanic carbon cycle and buffering of the global climate system (Deppeler and Davidson, 2017 and references therein).

2. Materials and Methods

2.1. Sampling and Locations

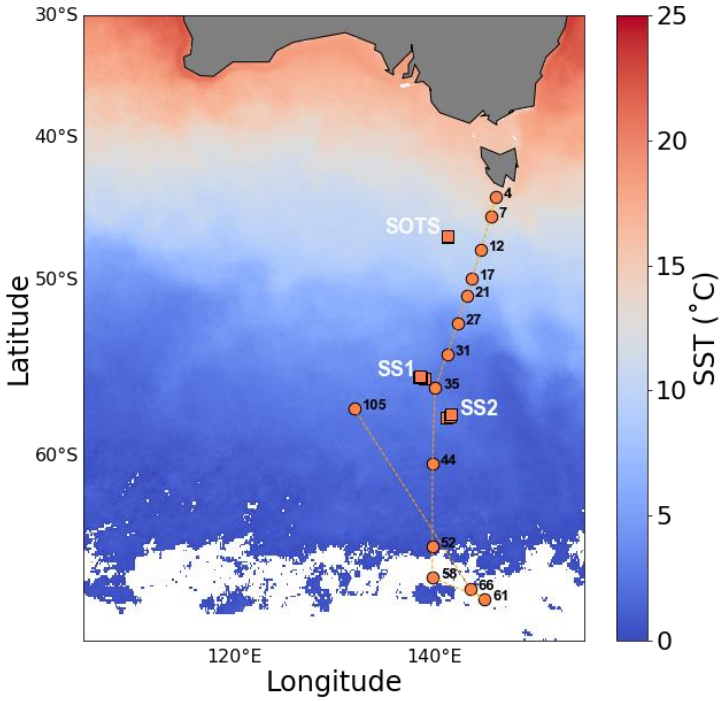

Figure 1. Annual mean Satellite Sea Surface Temperature (SST) map with station locations. SST is MODIS yearly product between 01/01/2021 and 31/12/2021. SR3 and SOLACE stations are marked by orange circles and squares, respectively. The SR3 voyage path is shown as orange dashed line.

Seawater samples were collected in the Australian sector of the Southern Ocean during *R.V. Investigator* voyages IN2018_V01 and IN2020_V08 (**Figure 1**). The IN2018_V01 voyage was part of a GEOTRACES expedition, which took place from 10 January to 22 February 2018 along the SR3 line (44°S – 66°S, 140°E – 146°E) from Hobart (Tasmania, Australia) to the Antarctic ice-edge. The IN2020_V08 voyage, part of the SOLACE (Southern Ocean Large Area Carbon Export) project, was conducted between 4 December 2020 and 15 January 2021. Sampling took place at three sites: the Southern Ocean Time Series (SOTS) site (47°S, 142°E) and two southern sites (SS1 and SS2), at approximately 55°S and 58°S, respectively. Diatom blooms were apparent at all three sites.

Seawater samples for dissolved Sr analysis were collected using 12 L Teflon-coated Niskin bottles mounted on a conductivity-temperature-depth (CTD) rosette. Seawater was collected unfiltered during the IN2018_V01 voyage, stored in 5 mL polypropylene (PP) vials, kept under

room temperature and acidified close to the time of analysis. The unfiltered sample is expected to have a minimal impact on the measurement of dissolved Sr concentration, given that the maximum particulate Sr concentration measured (100 nmol kg^{-1}) was minor compared to the concentration of dissolved Sr (~88 µmol kg^{-1}). Seawater collected during the SOLACE voyage was filtered through a 0.2 µm Millipore membrane using a syringe, acidified to pH <2, and refrigerated in the dark until analysis. In addition to the CTD samples, seawater samples from three trace metal rosette (TMR) casts during the SOLACE voyage were selected for cation concentration analysis. Hydrographic and biogeochemistry data, including nutrients (silicate, phosphate, nitrate + nitrite, nitrite and ammonium), alkalinity and dissolved inorganic carbon, are available for both voyages at https://www.cmar.csiro.au/data/trawler/. The hydrology and CTD nitrate data along the SR3 line are shown in **Figure 2**.

During the SOLACE voyage, samples for analyzing particulate Sr were obtained using six large-volume dual-head McLane pumps. These pumps, deployed at different water depths of up to 500 m, collected the seawater onto acid-clean 0.2 µm polyvinylidene fluoride (PVDF) filters with a diameter of 142 mm. Samples were freeze-dried and stored at −80°C until analysis. Particulates were dissolved by adding strong acid digestion (HNO_3:HCl:H_2O:HF 1:1:2:0.5). Post-digestion samples were evaporated to dryness and re-dissolved. The Sr content was then measured on the ICP-OES using the method described in section **3.3**.

2.2. Seasonal Dissolved and Particulate Sr Samples

Archived samples from the SOTS moorings were analyzed for seasonal variations in particulate and dissolved Sr concentrations. SOTS moorings consist of two deep ocean moorings, including the Southern Ocean Flux Station (SOFS) and the SAZ sediment trap mooring. Sediment trap samples were collected at 1000 m depth at SAZ moorings, and samples for our study were selected from the following periods: 2010 (September 2010 to July 2011), 2018 (March 2018 to February 2019) and 2020 (September 2020 to April 2021). Sampling occurred approximately once every one or two weeks over periods ranging from a half year to one year. Detailed methodologies and results for SAZ and SOFS moorings can be found in Wynn-Edwards *et al.* (2020a) and Eriksen *et al.* (2018), respectively. In brief, sediment trap samples come back in individual 250 mL cups, which were filled with a buffered brine of filtered seawater and

mercuric chloride as a preservative before deployment. Amongst other additions, the brine was enriched with strontium chloride ($SrCl_2$) to slow down the dissolution of Acantharia. After recovery, the cups are poured over a 1mm Nylon mesh to separate the contents into >1mm and <1mm fractions. The >1mm fractions are rinsed and archived refrigerated in buffered seawater (with no further addition of $SrCl_2$). The <1mm fractions are filtered, rinsed with Milli-Q water, dried and then homogenized and stored at room temperature.

Surface seawater samples filtered through 1mm mesh were selected from the specific periods, including 2010 (September 2010 to April 2011), 2018 (August 2018 to March 2019) and 2021 (April 2021 to May 2022) at SOFS moorings. These selected samples were also analyzed for dissolved Sr concentrations. Other parameters, such as nutrient concentrations, temperature, and salinity, as well as particle fluxes, were previously measured, and the results are available at https://portal.aodn.org.au/search.

Subsamples of post-processing storage solutions from the >1mm fractions were analyzed for dissolved Sr concentration, assuming complete dissolution of Acantharia during the long-term storage (>2 years). The Sr concentration in the >1mm fraction was converted to Sr flux based on the volume of the subsample and total post-processing storage solution, area of the sediment trap opening (0.5 m^2) and the duration of collection period. Subsamples (~2 mg) of the processed <1mm powders were dissolved in 1 mL of 2% HNO_3 and measured for Sr concentration. The weight of the sample and acid was monitored at each step, thus allowing for the back-calculation of Sr mass in the 2 mg subsample, with corrections for background seawater and brine (contained $SrCl_2$) Sr concentration. The Sr flux in the <1mm fraction was calculated based on the measured total mass flux and percentage of Sr mass to the total mass in the cup. The total Sr flux was represented as the sum of Sr flux in both size fractions. Sr fluxes shown below are expressed as atom fluxes. Atom flux can be converted to mineral fluxes by multiplying by the molecular weight of its most likely molecular form. These fluxes were used when discussing ballasting and total mineral flux export.

2.3. Cation Concentration Analysis

The concentrations of Na, Ca, Mg and Sr were measured on the inductively coupled plasma-optical emission spectrometer (ICP-OES) following the method provided by Steiner *et al.* (2020, 2021). In summary, seawater samples were diluted with 2% HNO_3 at a ratio of 1:80 and measured on the ICP-OES using a sample standard bracketing procedure. Typical operating conditions used for ICP-OES are summarized in **Table S1**. To prevent cross-contamination and salt build-up, the ICP-OES torch and cone were cleaned with 2% HNO_3 before the start of each run.

The sequence of analysis started with 15 analyses of the in-house standard collected from the first TMR at 200 m depth during the IN2020_V01 voyage to monitor the stability and precision of the ICP-OES. Each sample measurement consisted of 18 replicate reads with a reading time of 5 s per replicate, followed by a 30 s rinse before and after each measurement. Every sample was bracketed by the in-house standard diluted to the same ratio as the sample. Samples were analyzed as duplicates or triplicates. The intensity ratios for Sr/Mg and Ca/Mg for samples were corrected for drift based on the average intensity ratios of the bracketing standard. These ratios were then normalized to the actual concentration of the bracketing standard to obtain the concentration of the sample. The optimal spectral line was selected based on the precision of combined spectral lines of intensity ratios. By using intensity ratios, we can remove the uncertainties associated with fluctuations in sample uptake, instrument gas flows and plasma instabilities. Additionally, this method eliminates the effect of salinity variations on sample concentrations, assuming that Mg is conservative in the open ocean. All dissolved Sr concentrations were normalized to a salinity of 35.

The precision of the Sr and Ca concentrations in a single sample was determined by performing duplicate or triplicate measurements. The average precision is obtained by calculating the mean of all individual precisions across the entire data set during a voyage. Outliers exceeding 1.5 standard deviations of the mean concentration of the depth profile were removed. The mean precision (1σ) of measurements was 0.06% for Sr/Mg (0.05 $\mu mol\ kg^{-1}$) and 0.08% for Ca/Mg (8 $\mu mol\ kg^{-1}$) for both the SR3 line and SOLACE samples, and 0.4 $nmol\ kg^{-1}$ for particulate Sr concentration.

3. Results

3.1. Spatial and Vertical Distribution of Dissolved Sr

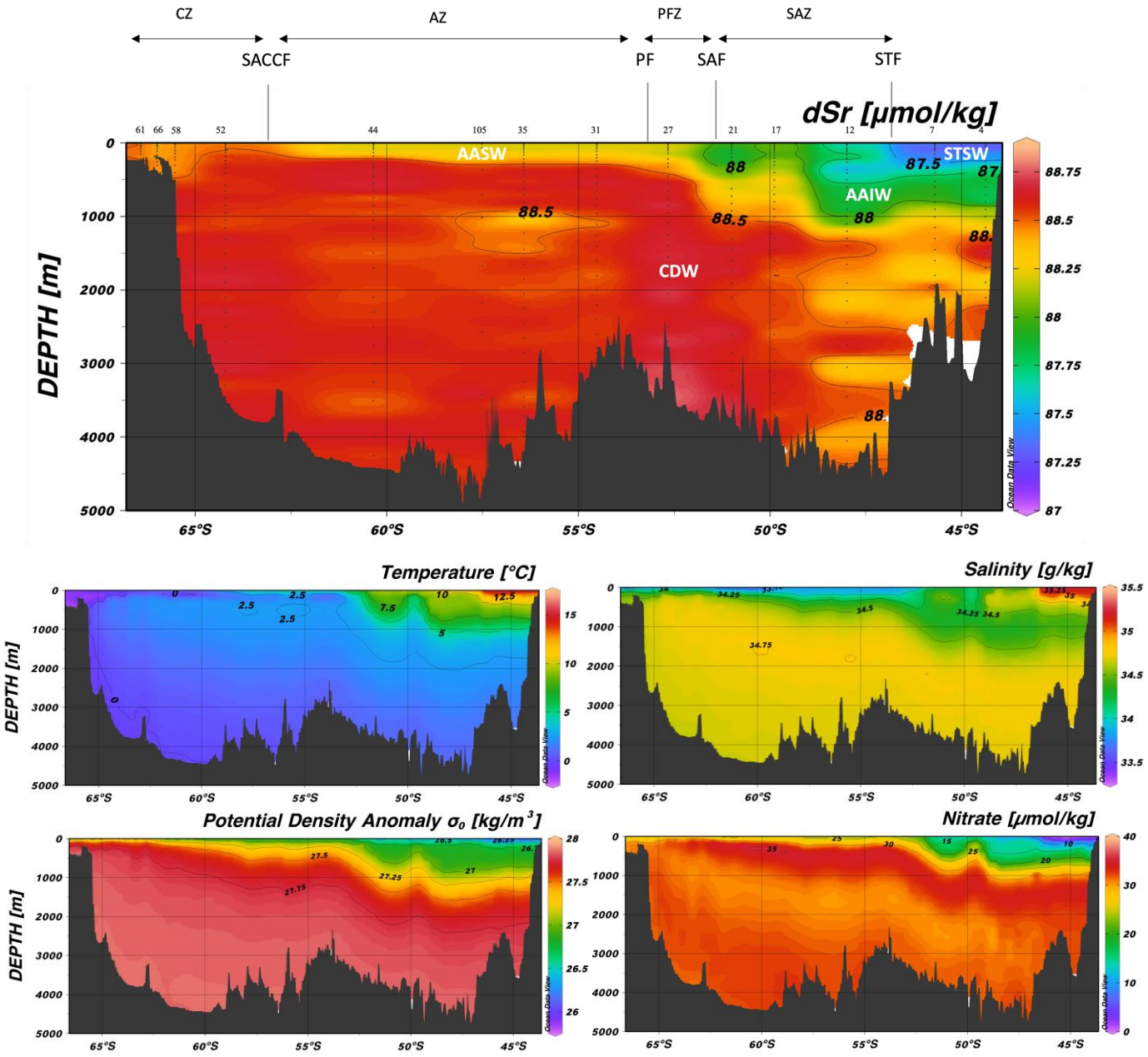

Figure 2. Salinity-normalised strontium concentrations, temperature, salinity, potential density anomaly, nitrate and oceanic fronts/zones along the SR3 line. The location of fronts and water masses are identified based on the description of Whitworth III and Nowlin Jr. (1987) and Orsi *et al.* (1995). Abbreviations: STSW: Subtropical Surface Water; AAIW: Antarctic Intermediate Water; AASW: Antarctic Surface Water; CDW: Circumpolar Deep Water; STF: Subtropical Front; SAF: Subantarctic Front; PF: Polar Front; SACCF: Southern Antarctic Circumpolar Front; SAZ: Subantarctic Zone; PFZ: Polar Frontal Zone; AZ: Antarctic Zone, CZ: Continental Zone. Ocean Data View software (Schlitzer, 2023) was used to generate this figure.

Along the SR3 line, salinity-normalized dissolved Sr (dSr) shows non-conservative behaviour with lower concentrations in surface waters and higher concentrations at depth (**Figure 2**). There was a noticeable difference in surface dSr concentrations from north to south, with values increasing from 87.3 µmol kg^{-1} near Tasmania to 88.5 µmol kg^{-1} near Antarctica. The lowest dSr concentration was observed at stations 4 and 7, which were located in the Subtropical Surface Water (STSW) of the subtropical gyre. Additionally, a stronger vertical gradient in dSr concentrations was found in the Subantarctic Zone (SAZ) and further north, indicating a depletion of surface dSr relative to deep waters of up to 1.4%. Finally, deep waters below 1500 m were homogenously well-mixed and characterized by a high dSr concentration: 88.4 µmol kg^{-1} in SAZ and 88.6 µmol kg^{-1} south of the SAZ due to the upwelling of Circumpolar Deep Water (CDW) enriched in dSr.

The distribution of dSr for the SOLACE voyage was similar to dSr determined along the SR3 line **(Figure 3a**). dSr depletion occurred to a deeper depth at SOTS compared to southern sites. At SOTS, the surface dSr was depleted by 0.8 µmol kg^{-1} relative to deep waters, and the maximum dSr concentration was observed at depths between 1250 and 2000 m. Whereas, at SS1 and SS2, the surface dSr was depleted by 0.45 µmol kg^{-1} relative to deep waters, and the maximum dSr concentration was observed at a shallower depth of approximately 500 m.

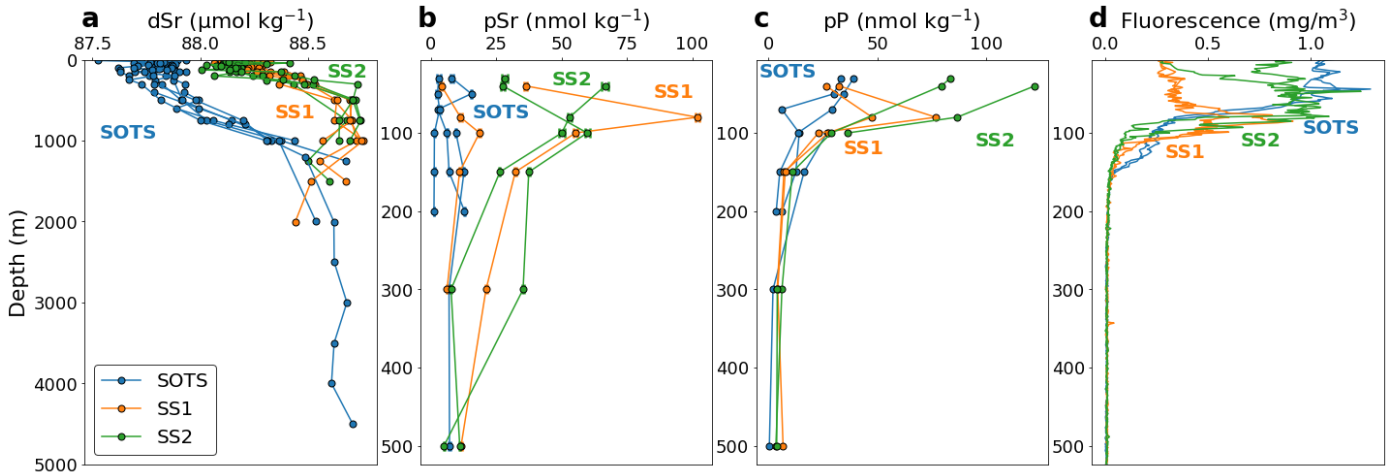

Figure 3. Depth profiles of salinity-normalised dissolved strontium (a), particulate Sr (b) and particulate phosphate (c) and fluorescence (d). The samples were collected during SOLACE voyage at three main stations: SOTS, SS1 and SS2. The average precision of salinity-normalised dissolved Sr concentrations is 0.05 $\mu mol\ kg^{-1}$, and for particulate Sr is 0.4 $nmol\ kg^{-1}$ (1σ). Note the difference in the depth scales between panel a, and b, c and d.

The vertical distribution of particulate Sr (pSr) concentration at SS1 and SS2 exhibited a subsurface maximum at approximately 100 m before decreasing rapidly with depth (**Figure 3b**). Interestingly, pSr concentrations at SS1 increased significantly between the first and second sampling, with values going from 25 nmol kg^{-1} to 100 nmol kg^{-1} at 100 m. An increase in particulate phosphate (pP) was also observed at this station (**Figure 3c**). For SS2, pSr concentrations at 100 m were similar between stations. In contrast to SS1 and SS2, pSr concentrations at SOTS were generally lower, with values consistently below 17 nmol kg^{-1} and without any apparent sub-surface maximum. The trend of pSr at SS1 and SS2 closely resembled that of pP and fluorescence concentrations (**Figure 3c and 3d)**, with maximum concentration occurring at the same depth.

3.2. Seasonal Pattern of Dissolved and Particulate Sr

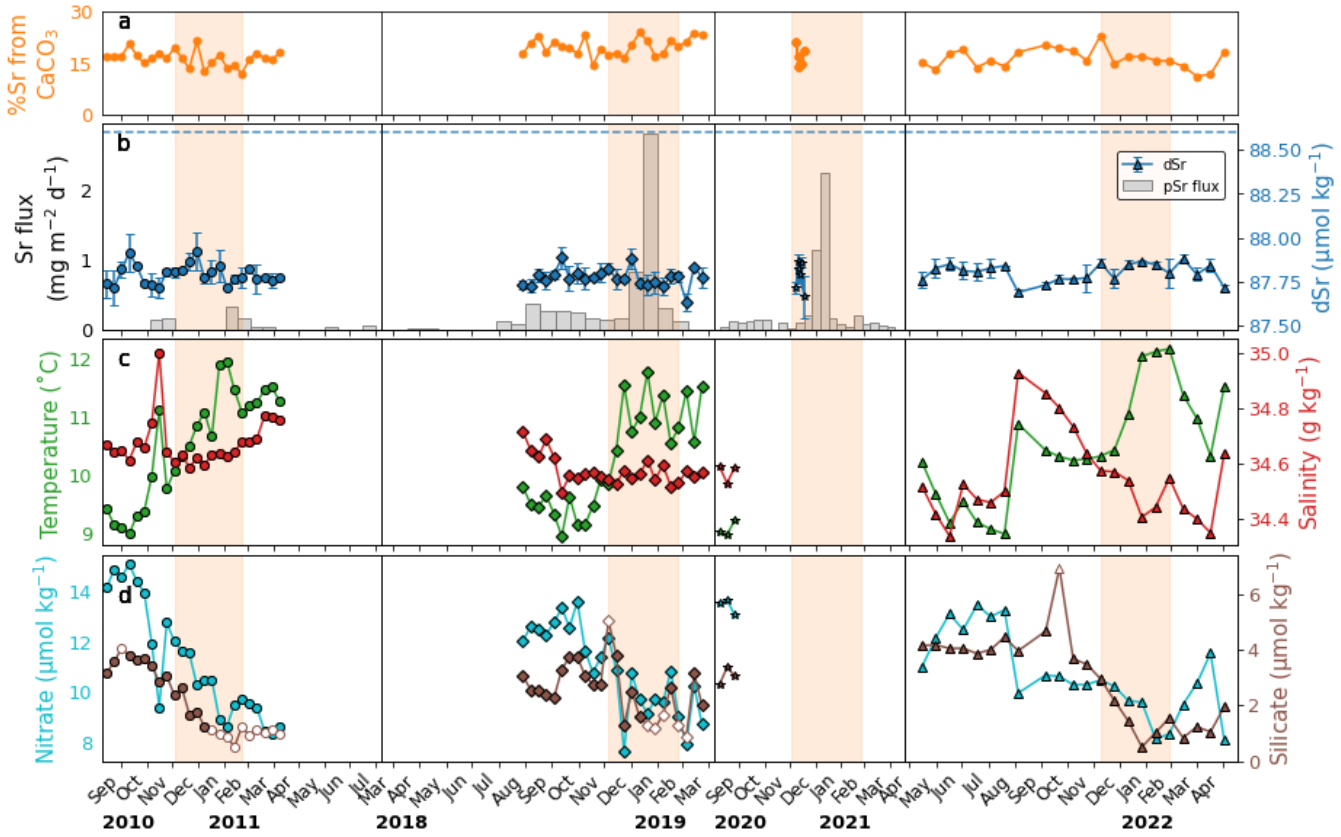

Figure 4. Seasonal variations in particulate Sr fluxes at 1000 m depth and surface biogeochemical parameters. The plot represents data obtained from four mooring deployments: September 2010 to July 2011, March 2018 to March 2019, September 2020 to April 2021 and May 2021 to May 2022. Vertical black solid lines mark the approximate end time of each deployment. Panel a shows the percentage contribution of $CaCO_3$ (based on dissolved Ca) to the change surface and deep waters to the change in dissolved Sr (dSr). Panel b shows the total particulate Sr (pSr) export fluxes (combined >1mm and 1<mm fluxes) from SAZ moorings (grey bars), alongside dSr concentrations in surface water from SOFS moorings (blue line). The blue dashed line indicates the average dSr concentration in deep waters (>3000 m). Panel c exhibits seasonal sea surface temperature and salinity patterns, while the panel d illustrates nitrate and silicate seasonal variations. For panel d, filled shapes indicate good data quality (flag = 1), while open shapes suggest less reliable data (flag >1) and should be interpreted cautiously. Circles (2010), diamonds (2018), stars (2020) and triangles (2021) represent surface biogeochemical measurements in the corresponding deployment years. Summer (December to February) is shaded light orange each year. Notably, there is a data gap for biogeochemical data in 2020 and sediment trap data in 2021. Most of the pSr flux data is unavailable for 2010. The %Sr from $CaCO_3$ and dSr for 2020 was determined based on dSr and dCa data measured during SOLACE voyage at SOTS.

Seasonal variability in dSr at SOTS was relatively low, with a constant surface concentration of 87.18 ± 0.08 µmol kg^{-1}, which was consistently lower than that in deep waters (~88.6 µmol kg^{-1}) (**Figure 4**). Any observed variations in dSr occurred during the incursion of saltier, warm subtropical waters into fresher subantarctic waters in the spring of 2010 and 2021. This mixing resulted in a reduction in dSr concentration by 0.1 – 0.15 µmol kg^{-1}. Conversely, the pSr

247 flux recorded in the 1000 m sediment trap displayed a pronounced seasonal pattern in 2018 and
248 2020. The pSr flux peaked in January/February at a maximum of 2.8 and 2.2 mg Sr $m^{-2}d^{-1}$ in
249 2018 and 2020, respectively. The pSr flux decreased rapidly after the peak and remained below
250 0.4 mg Sr $m^{-2}d^{-1}$ for the rest of the year. Nitrate and silicate also showed seasonal variations
251 consistent with drawdown by phytoplankton from spring through to summer.

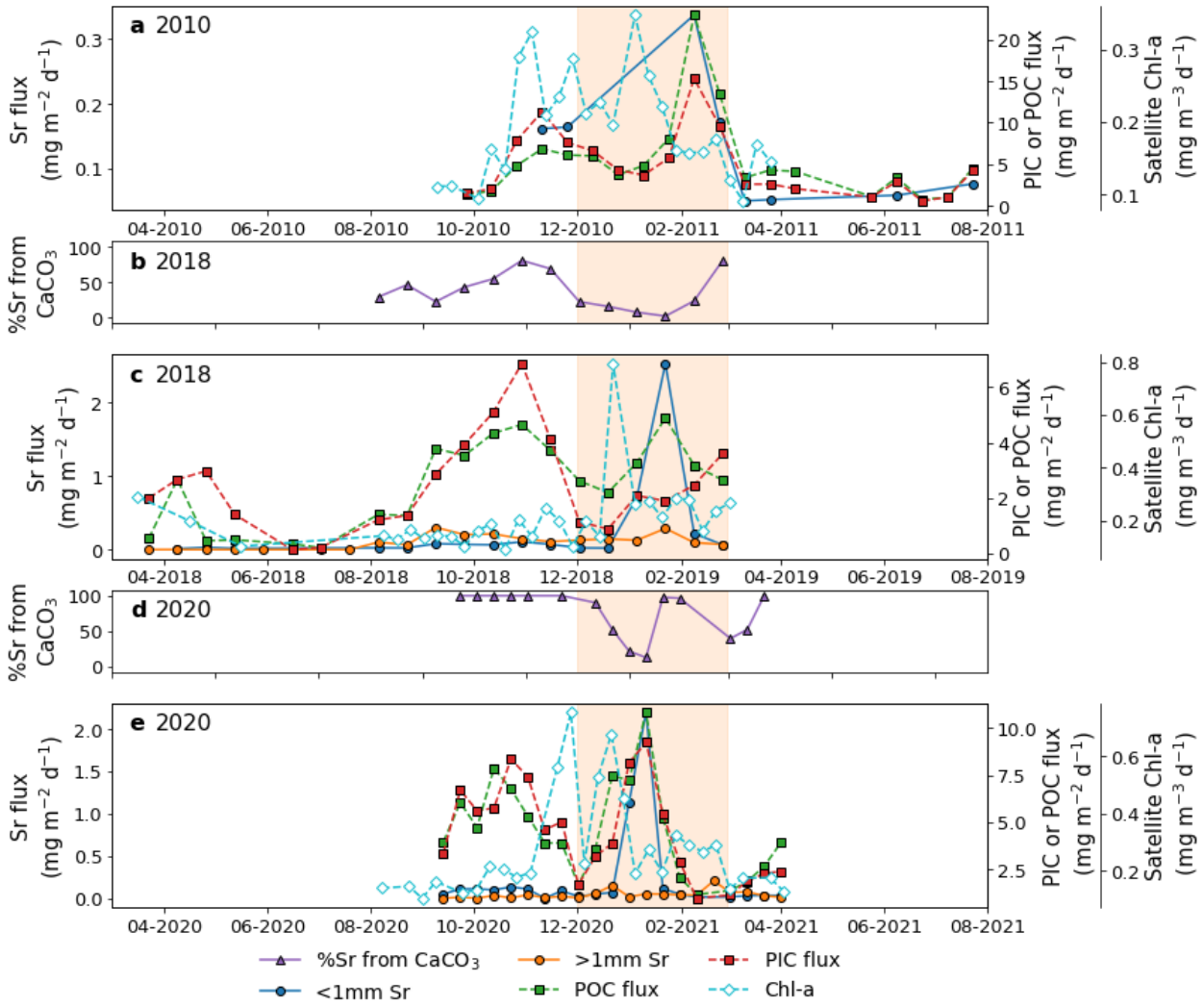

Figure 5. Fluxes of particulate Sr, PIC and POC from the 1000 m sediment trap and satellite chlorophyll a concentration across the sampling year. Panels b and e show the percent contribution of $CaCO_3$ (aragonite : calcite = 0.54) flux to particulate Sr (pSr) flux. The contribution was computed when data for both <1mm and >1mm fractions were available, and it was excluded for pSr flux values less than or equal to 0.05 $mg\ Sr\ m^{-2}d^{-1}$ due to significant overestimation. Additionally, any contribution exceeding 100% was capped at 100%. pSr flux (a, c and e) was subdivided into <1mm and >1mm fractions. No >1mm fraction was measured for Sr concentration in 2010 and there was missing data in <1mm fraction in 2010. The mean uncertainty of pSr flux across the dataset is 0.006 $mg\ Sr\ m^{-2}d^{-1}$. It is important to note that the y-axis scale is not consistent in each panel. Chlorophyll a data, obtained from MODIS-Aqua 8 days product, was averaged in the -45 to -48°S and 141 – 143°E zone across the sampling year. Summer (December to February) is shaded light orange each year.

Seasonal pSr fluxes at 1000 m were dominated by the <1mm size fraction, with the >1mm generally representing less than 2% of the flux (**Figure 5**). Most of the pSr flux occurred in January/February, but there was still measurable export throughout the year, ranging from 0.008 to 2.8 mg Sr $m^{-2}d^{-1}$, with an annual mean of 0.31 ± 0.6 mg Sr $m^{-2}d^{-1}$. Conversely, the pSr

flux from the >1mm fraction remained consistently low at 0.07 ± 0.08 mg Sr $m^{-2}d^{-1}$ throughout the year, with a small peak of 0.3 mg Sr $m^{-2}d^{-1}$ in September 2018.

A comparison of particle fluxes registered at the sediment trap indicates that the total mass flux was dominated by $CaCO_3$, POC and opal (**Figure S2**). The fluxes for these major components displayed two peaks: a broad, moderate peak occurred during spring (September – November) and a second, shorter, more intense peak in summer (January/February) (**Figure 5**) (see Cathryn A. Wynn-Edwards *et al.*, 2020a for a detailed description of this seasonality from long-term SAZ data). However, the pSr flux was characterized by only one intense export event in summer, coinciding with the second peak in the POC flux. Despite POC fluxes being 4-fold and 2-fold higher than in 2010 compared to 2018 and 2020, respectively, the corresponding pSr flux peak was lower in 2010 (~0.34 mg Sr $m^{-2}d^{-1}$) compared to 2018 (2.5 mg Sr $m^{-2}d^{-1}$) and 2020 (2.8 mg Sr $m^{-2}d^{-1}$). A comparison of surface ocean productivity (as indicated by satellite chlorophyll *a* concentration) and other particle fluxes registered by the sediment trap suggests that high productivity was associated with the later peak in summer.

4 Discussion

4.1. The Role of Acantharia in Strontium Cycling

The depletion of dSr in the upper ocean and the close correlation of pSr with pP imply that Sr removal from the upper ocean is biologically mediated. Acantharia emerge as the primary driver, as they are the only organisms that produce an entire skeleton of $SrSO_4$ in the ocean (Decelle and Not, 2015). Although there is a potential for Sr removal through $CaCO_3$ production, particularly in the 'Great Calcite Belt' near the SAZ where $CaCO_3$ production is significant (Balch *et al.*, 2011, 2016), caution is warranted. The contribution from $CaCO_3$ may be limited, considering the tendency for satellite-derived PIC in the Southern Ocean to be overestimated (Trull *et al.*, 2018). Using the Ca concentration observed at SOFS moorings, assuming aragonite constitutes 35% of the total $CaCO_3$ production (Gangstø *et al.*, 2008) and applying a Sr/Ca ratio of 0.0015 mol mol^{-1} in biotic calcite and 0.009 mol mol^{-1} in biotic aragonite (Steiner *et al.*, 2020 and references therein), $CaCO_3$ production is estimated to contribute approximately 17% to surface

Sr removal averaged across sampling years (**Figure 4**). This further emphasizes that Acantharia is the primary driver of dSr in the Southern Ocean.

Investigating $CaCO_3$ contribution to pSr flux revealed that the background pSr was influenced by $CaCO_3$, while Acantharia dominated during peak pSr events. Applying consistent aragonite/total $CaCO_3$ and Sr/Ca ratios in calcite and aragonite, $CaCO_3$ predominantly controlled the pSr flux in non-productive seasons, contributing an average of 49% and 88% for 2018 and 2020, respectively (**Figure 5b and 5d**). This contribution from $CaCO_3$ to the pSr flux at 1000 m significantly exceeded the contribution calculated from dCa to dSr in the surface water (**Figure 4**). The disparity was attributed to the dissolution of pSr on the way to the trap, as $SrSO_4$ is more soluble than $CaCO_3$ in seawater, leaving the $CaCO_3$ to dominate the background pSr flux. Comparing the model-estimated pSr export leaving 200 m at 1.7 ± 0.3 mg Sr $m^{-2}d^{-1}$ (**Table 2**) and the average sediment trap-registered pSr flux at 1000 m of 0.25 mg Sr $m^{-2}d^{-1}$, it is suggested that up to 85% of the pSr was dissolved between 200 m and 1000 m, exceeding PIC dissolution (64%) based on our model estimates and the 1000 m trap flux. pSr flux was not tightly coupled with PIC flux, especially during the productive season. The PIC export flux exhibited two peaks annually, contrasting with the single pSr peak in summer. Despite lower PIC flux in 2018, pSr flux was higher than in 2020. Notably, $CaCO_3$ contributed only 2% and 12% to the pSr peak in 2018 and 2020, respectively. These findings indicate that Acantharia-derived $SrSO_4$, rather than $CaCO_3$, was the major contributor to the pSr peaks. The dominance of the <1mm fraction in pSr flux (**Figure 5**), aligns with observations of Acantharia's smaller size in the Southern Ocean (<500 μm) (Spindler and Beyer, 1990; Gowing and Garrison, 1992; Belcher *et al.*, 2018), further supporting the notion that pSr peak was governed by Acantharia.

Correcting $CaCO_3$ contribution to pSr flux yielded a nearly unchanged Acantharian Sr flux in 2018 at 2.8 mg Sr $m^{-2}d^{-1}$ and slightly reduced it from 2.3 to 2.0 mg Sr $m^{-2}d^{-1}$ in 2020. pSr fluxes were converted to POC fluxes using an Acantharia C:Sr ratio of 0.12 ± 0.022 reported by Martin *et al.* (2010) from the Iceland Basin at 2000 m. When compared to the total POC flux, the maximum Acantharia contribution (corrected for $CaCO_3$-derived Sr) to total POC export was 6.8% and 2.2% in 2018 and 2020, respectively (**Figure S1**).

4.2. Acantharia Spatial and Vertical Distribution in the Southern Ocean

Acantharia play a significant role in the vertical and spatial distribution of dSr in the Southern Ocean. They remove Sr from the surface waters to build skeletons and form cysts, subsequently releasing it back into the water column at intermediate depths upon their death (Brass and Turekian, 1974; de Villiers, 1999; De Deckker, 2004; Steiner *et al.*, 2020). The observed depth of maximum dSr indicates that Acantharia dissolution primarily occurs around 1000 m in the SAZ and further north, which contrasts with Antarctic waters, where dissolution occurs at shallower depths of no deeper than 500 m (**Figure 3a**). These findings are consistent with the recent study by Steiner *et al.* (2020) conducted in the Indian Ocean sector of the Southern Ocean.

Our pSr concentrations show that Acantharia were most prevalent in the euphonic zone with a rapid decline below 100 m (**Figure 3c**). This trend aligns with findings from previous Southern Ocean studies, indicating the highest abundance of Acantharia within the upper 300 m (Spindler and Beyer, 1990; Gowing and Garrison, 1992; Henjes *et al.*, 2007; Jacquet *et al.*, 2007). Furthermore, our dSr concentration data shows that the majority of Acantharia dissolved in the upper 500 m of polar waters, indicating their habitat was confined to this depth range. The pSr was positively correlated with pP concentration (slope = 0.48, R^2 = 0.36, $p < 0.001$), and the maximum pSr, pP and fluorescence concentrations occurred at the same depth (**Figure 3c and 3d**). This suggests that pSr concentration likely represents the abundance of living Acantharia, which were actively feeding on plankton (Henjes *et al.*, 2007; Jacquet *et al.*, 2007). Additionally, Acantharian clades E and F may be present, previously identified in the Southern Ocean (Gowing and Garrison, 1992; Henjes *et al.*, 2007; Assmy *et al.*, 2014). These Acantharia host symbiotic algae and inhabit the euphotic zone throughout their life cycle due to the requirement of their symbionts for light (Michaels, 1988, 1991; Decelle *et al.*, 2012).

4.3. 2-D Modelling of Sr Fluxes in the Southern Ocean

Despite salinity normalization of dSr removing some mixing effects, the dSr distribution may still be influenced by ocean circulation. For instance, the strong upwelling of CDW can homogenize the dSr concentration in the polar and subpolar waters and result in a shallower maximum of dSr. Conversely, the subduction of Antarctic Intermediate Water (AAIW) and Subantarctic Mode Water (SAMW) north of the Polar Front (PF) transfers a low dSr signal down

to 1000 m, resulting in a deeper maximum dSr. To assess and eliminate the impact of ocean circulation on Sr fluxes, a two-dimensional model was applied to our dSr data (**Figure 6**). The model serves as an independent tool to the sediment trap flux data to evaluate pSr export fluxes in the upper 200 m, and it allows for comparative analysis among different zones in the Southern Ocean.

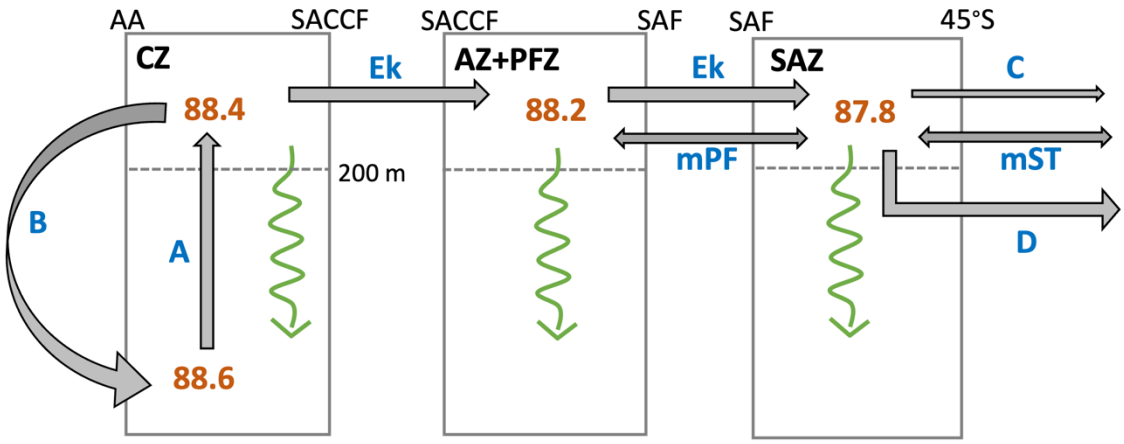

Figure 6. Schematic diagram of a 2-D ocean circulation model in the Southern Ocean. Water transports are denoted by grey arrows. pSr export fluxes are represented by green wave-shaped arrows. Sr concentration, measured in $\mu mol\ kg^{-1}$, is shown in orange. Abbreviations: SAZ: Subantarctic Zone; AZ+PFZ: Antarctic Zone + Polar Frontal Zone; CZ: Continental Zone. SAF: Subantarctic Front; SACCF: Southern Antarctic Circumpolar Front; AA: Antarctica.

Table 1

Description and Range or Conditions of Parameters in 2-D Model

Parameters	Description	Range/Conditions (Sv)
A	Upwelling from CDW	A = 24
B	Dense water formation	B = 16
Ek	Ekman transport	Ek = 8
mPF	Mixing between SAZ and PFZ	0<= mPF <= 3.97
mST	Mixing between STZ and SAZ	0<= mST <= 8.23
C	Flux towards low latitude surface	C = 2
D	Intermediate and mode water formation	D = 6

Note. Water flux values are taken from Talley (2013).

The water mass transport values were obtained from Talley (2013), and mixing terms (mPF and mST were introduced for PFZ and SAZ to account for horizontal mixing between PFZ and SAZ and SAZ and STZ (**Table 1**). The upper bounds of mixing terms were determined by the mass balance of Sr flux in each zone, ensuring that the mass balance remains non-negative. The Sr fluxes were converted to carbon fluxes using a C:Sr ratio of 0.12 ± 0.022 mg mg^{-1} (Martin *et al.* 2010). The annual POC flux leaving the upper 200 m was estimated using the nitrate flux and Redfield Ratio of 106 C: 16 NO_3^- (Johnson *et al.*, 2017). Comparisons between Sr-derived carbon flux and nitrate-derived biological carbon flux were made to determine the percentage contribution of Acantharian cysts to annual POC flux in the Southern Ocean.

The maximum modelled pSr export fluxes were similar (within errors) across all zones, with the highest in the CZ at 2.2 ± 1.0 mg Sr $m^{-2}d^{-1}$, slightly less in the SAZ at 1.7 ± 0.3 mg Sr $m^{-2}d^{-1}$ and lowest in the AZ+PFZ at 1.1 ± 0.3 mg Sr $m^{-2}d^{-1}$ (**Table 2**). When accounting for an attenuation factor of 0.858 for pSr flux (Martin *et al.*, 1987), the pSr flux at 200 m at SOTS estimated from the mean pSr flux at 1000 m across sampling years is 1 mg Sr $m^{-2}d^{-1}$. This result is lower than the maximum pSr fluxes in the SAZ under maximum mPF and minimum mST conditions. However, it is important to note that the modelled pSr and POC fluxes are highly dependent on the choice of water mass transport values, which may exhibit a large amount of uncertainty. Additionally, the advection of subtropical waters along the Antarctic Circumpolar Current (ACC) is estimated to contribute to a POC export flux of 1.25 mol C $m^{-2}yr^{-1}$ in the SAZ (Fernández Castro *et al.*, 2022). This is comparable to the model-estimated POC export flux of 1.1 mol C $m^{-2}yr^{-1}$ from the euphotic zone (**Table 2**), suggesting the model result serves as an upper limit for pSr and POC export flux in the surface SAZ.

Table 2

Model Results of Acantharian Flux, Acantharian Carbon Contributions and Total Carbon Flux in Upper 200 m in the Southern Ocean Zones

Zone	Area (m^2)	Value of dominant parameter (Sv)	Surface Sr ($\mu mol\ kg^{-1}$) [#]	Maximum Acantharian flux (mg Sr $m^{-2}\ d^{-1}$) [¥]	Acantharian carbon flux (mg C $m^{-2}\ d^{-1}$) [¥]	Contribution to annual POC flux (%) [¥]	NO_3^- concentration ($\mu mol\ kg^{-1}$) [&]	Annual POC flux (mg C $m^{-2}\ d^{-1}$) [&]	Annual POC flux (mol C $m^{-2}\ yr^{-1}$) [&]
CZ	1.22×10^{13}	A = 24	88.46 ± 0.04 [‖]	2.2 ± 1.0	0.26 ± 0.12	0.8 ± 0.4	29.56 ± 0.01 [‖]	33.31 ± 0.19	1.013 ± 0.006
AZ+	1.22×10^{13}	mPF = 6.18	88.24 ± 0.04 [§]	0.0	0	0	27.12 ± 0.01 [§]	0	0
PFZ		mPF = 0		1.1 ± 0.3	0.13 ± 0.04	1.2 ± 0.4		11.00 ± 0.06	0.335 ± 0.002
SAZ	2.44×10^{13}	mST= 7.12, mPF = 0	87.79 ± 0.05 [¶]	0.0	0	0	15.62 ± 0.01 [¶]	0	0
		mST = 0, mPF = 6.18		1.7 ± 0.3	0.20 ± 0.05	0.5 ± 0.1		36.56 ± 0.05	1.112 ± 0.001

Note. [#] The surface dSr concentration represented the average dSr concentration in the upper 200 m. The dSr concentration in Circumpolar Deep Water was 88.6 ± 0.05 μmol kg^{-1}, averaged below 3000 m depth. dSr in the STZ was 87.33 ± 0.03 μmol kg^{-1}. For the STZ dSr concentration, stations 4 and 7 from SR3 were chosen.

[‖] For the CZ dSr and NO_3^- concentration, stations 58, 61 and 66 from SR3 were selected.

[§] For AZ+PFZ, stations 31,35 and 105 from SR3 were selected.

[¶] For SAZ, stations at SOTS from SOLACE were chosen.

[¥] The errors of both Acantharian fluxes and contributions (1σ) were determined based on the errors of dSr, NO_3^-concentrations and C:Sr ratio.

[&] The NO_3^- concentrations represent the value at approximately 100 m as NO_3^- regeneration occurs below this depth.

4.4. Decoupling of Surface dSr and Sr Fluxes at 1000 m

The surface dSr concentration at the SOTS site remained relatively constant throughout the year, showing a decoupling from the apparent seasonality observed in pSr fluxes at 1000 m (**Figure 4**). One potential explanation was that horizontal mixing homogenized surface dSr concentrations. To test this hypothesis, we applied the 2-D model to the observed Sr fluxes from sediment traps at 1000 m, where adjustments were made to the mixing terms (mST and mPF) to align the modelled dSr with the observed concentration while keeping other parameters constant. Using this approach, we found that most variations in dSr could be eliminated by adjusting the mixing terms (**Figure S3)**. However, when pSr fluxes were notably high, such as in the summer of 2018 and 2020, the model consistently yielded a lower dSr compared to observations by 0.2 – 0.3 $\mu mol\ kg^{-1}$, even with adjustments to the mixing terms. Moreover, the model yielded mean values of 7 and 0.6 Sv for mST and mPF across the sampling years, resulting in a pSr flux in the SAZ at 200 m of 0.24 $mg\ C\ m^{-2}d^{-1}$, considerably lower than the estimated Sr flux of 1 $mg\ C\ m^{-2}d^{-1}$ from the sediment traps.

The observed decoupling between dSr and sediment traps suggests that factors beyond mixing may contribute to these discrepancies. One plausible explanation is that the potential difference in integration times is represented by dSr and sediment trap-derived pSr. dSr reflects the long-term integration of Sr cycling processes. Changes in dSr occur on the hundreds to thousands of year time scale due to the long residence time of dSr in the ocean (**Figure S4**). This prolonged residence time hinders the detection of any discernible seasonal changes in dSr. Conversely, sediment trap-derived pSr fluxes are snapshots of a particular stage in the dSr seasonal cycle, representing weekly/monthly means. Moreover, the growth and increase in the population of Acantharia may take months, while the senescence and sinking could occur in a few days. This suggests that the time required for mixing to replenish dSr is likely longer than the duration of peak pSr fluxes to the traps. Additionally, the impact of pSr on dSr concentration was limited, with a maximum measured value (100 nmol kg^{-1}) contributing minimally (~0.1%) compared to the concentration of dSr (~88 μmol kg^{-1}). It is important to emphasize that sediment traps might capture surface collection over a broad region due to eddy and mean flow advection (Siegel and Deuser, 1997), potentially leading to inaccurate particle flux measurements.

4.5. The Contribution of Acantharia to Downward Particle Flux

The relative importance of Acantharia in export fluxes at 200 m compared to calcareous plankton was assessed by analyzing the slope of the linear regression between dissolved Ca and Sr concentrations. For SR3 samples, the slope was 0.016 (R^2 = 0.83), and a similar slope was obtained from SOLACE samples at 0.012 (R^2 = 0.78) (**Figure 7**). Assuming a Sr/Ca ratio of 0.0015 mol mol^{-1} in biotic calcite and 13.6 mol mol^{-1} in celestite (Steiner *et al.*, 2020), this suggests that the contribution of $SrSO_4$ produced by Acantharia to the total amount of $CaCO_3$ + $SrSO_4$ export fluxes was 1.4% and 1% for SR3 and SOLACE samples, respectively. In other words, this indicates that Acantharia's role in the export flux was significantly less pronounced compared to calcareous plankton in the study region. This is supported by the sediment trap results, which showed that annual mass flux at 1000 m was mainly composed of $CaCO_3$ (65%), while $SrSO_4$ made up, on average, ~1% of material captured in the traps (**Figure S2**).

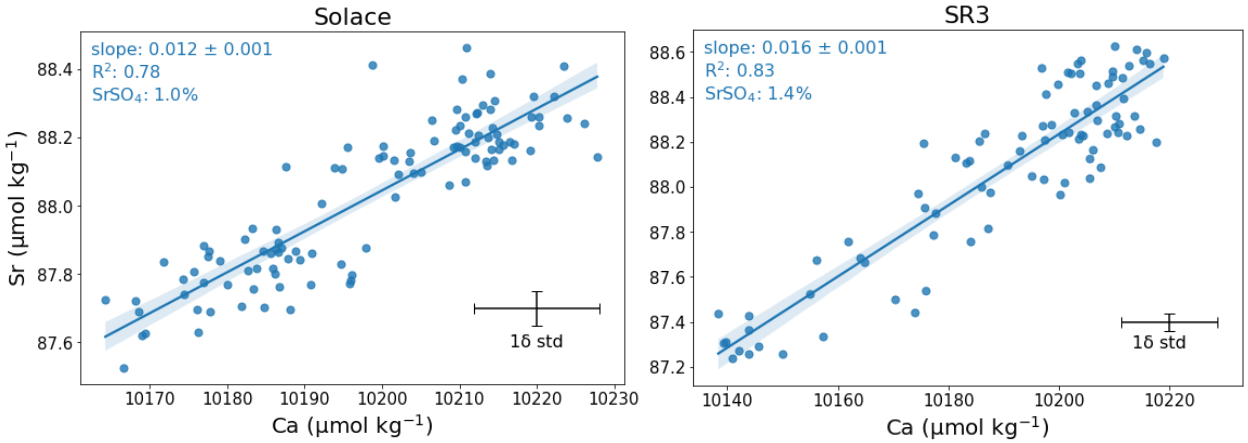

Figure 7. Salinity-normalised Ca and Sr concentrations from SOLACE and SR3 voyages for 0 – 100 m. Regression line is denoted by a blue solid line. The top-left corner displays the slope and its associated error, the R-squared value, and the percentage of $SrSO_4$ relative to the total $SrSO_4$ + $CaCO_3$ flux. The 1σ standard deviation of the individual data points is depicted at the bottom-right corner of the plot.

Both the model-derived and sediment trap-derived Acantharian POC fluxes suggest their annual contribution to the total POC flux was negligible (~1%). Nevertheless, sediment trap measurements might underestimate pSr flux, primarily because only preservatives were measured for dSr concentration in >1mm fractions, potentially leaving undissolved Acantharia in samples, especially during periods of high Acantharia flux that could prevent further dissolution due to elevated dSr concentration in the preservative (Belcher *et al.*, 2018). Moreover, for <1mm

fractions, only particulates were measured for dSr concentration, potentially resulting in an underestimation of the flux value due to possible dissolution or fragmentation during the sediment trap deployment period, despite the addition of $SrCl_2$ to the preservative (Bernstein *et al.*, 1987; Wynn-Edwards *et al.*, 2020b).

Although the annual mean contribution of pSr fluxes to POC fluxes was generally low, their contributions became more pronounced during the productive season, as observed in the summers of 2018 and 2020 in this study, with a maximum contribution of ~7% to POC flux. This seasonal pattern aligns with findings in other high latitude studies, and the maximum Acantharian POC fluxes (0.33 $mg\,C\,m^{-2}d^{-1}$) registered at 1000 m fall within the range estimated by these previous investigations (**Figure 8**). Martin *et al.* (2010) reported elevated Acantharian POC fluxes of 0.45 $mg\,C\,m^{-2}d^{-1}$ at 2000 m during a spring bloom in the Iceland Basin, which accounted for up to 48% of the POC export flux. However, considering the annual POC flux, the contribution of Acantharia in the Iceland Basin is likely to remain relatively low (<1-2 %), due to minimal Acantharian fluxes at other times. Similarly, Decelle *et al.* (2013) and Belcher *et al.* (2018) measured Acantharian fluxes in the Scotia Sea at 1500 m and 2000 m, respectively. They found higher Acantharian fluxes in austral summer and significantly lower fluxes at other times of the year. However, Decelle *et al.* (2013) reported a much lower maximum Acantharian POC flux of 0.14 $mg\,C\,m^{-2}d^{-1}$ compared to 5.11 $mg\,C\,m^{-2}d^{-1}$ reported by Belcher *et al.* (2018). This indicates that the magnitude of Acantharian fluxes varies from year to year. Moreover, the Decelle *et al.* (2013) study likely underestimated pSr flux as only preservatives were measured. Additionally, the high Acantharian fluxes observed by Belcher *et al.* (2018) are likely associated with unusually high POC fluxes, reaching a peak of 30 $mg\,C\,m^{-2}d^{-1}$ in December, surpassing values observed in the study of Decelle *et al.* (2013) at ~4 $mg\,C\,m^{-2}d^{-1}$.

4.6. The Role of Acantharia in POC Export

The unexpected co-sedimentation of Acantharia and POC at 1000 m traps contradicts the observed sequence where cyst formation precedes POC blooms. This sequence is hypothesized to result from the need of swarmers and juveniles to escape predation and access to higher

nutrient and organic matter concentrations (Spindler and Beyer, 1990; Martin *et al.*, 2010; Decelle *et al.*, 2013). The simultaneous peak of all particles implies that they were exported in the form of aggregates (Honjo *et al.*, 2008; Boyd *et al.*, 2019), suggesting a potential role for Acantharia in contributing to POC export through ballast. The denser Acantharian shells or skeletons (3.96 g cm^{-3}), compared to the dominant ballast of diatom frustules (2.65 g cm^{-3}) or coccoliths (2.71 g cm^{-3}) in the SAZ, positions Acantharia as an effective ballast for POC export through rapid sinking (Martin *et al.*, 2010; Decelle *et al.*, 2013). Based on observed particle fluxes and their respective densities, Acantharia have the potential to elevate the density of total ballast (composed of $SrSO_4$, SiO_2, and $CaCO_3$) by up to 11% during the productive season.

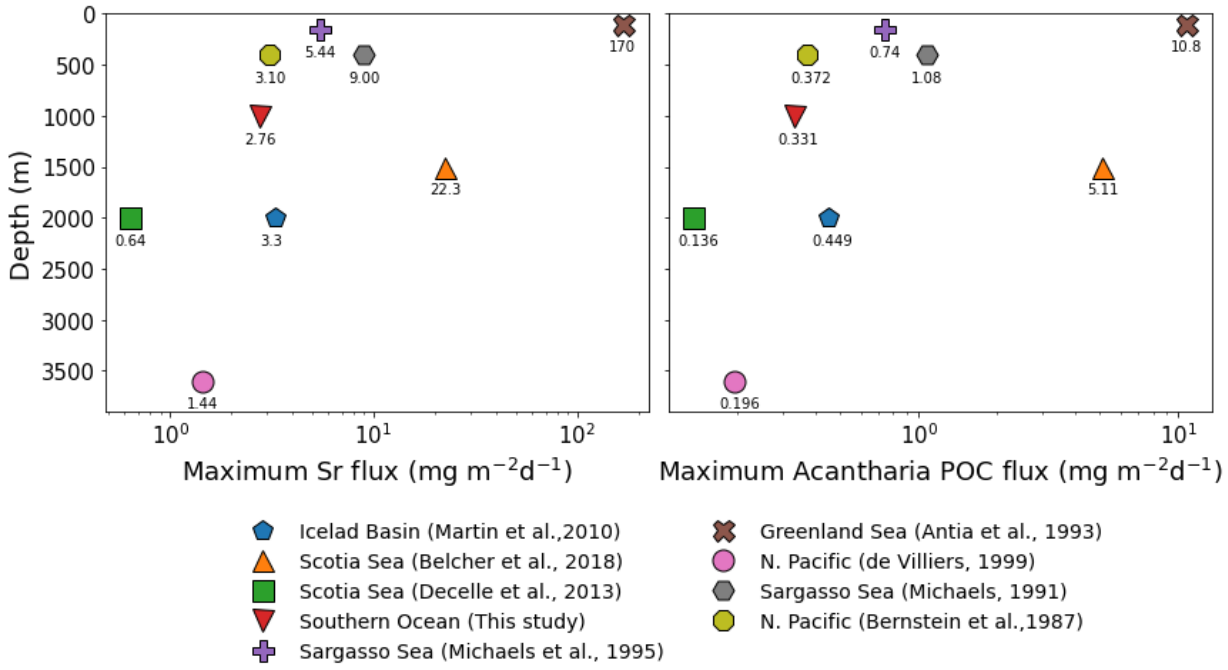

Figure 8. Comparison of maximum Sr (left) and Acantharian-associated POC (right) fluxes from our sediment trap data to published literature values. Both Sr flux and Acantharian POC flux were corrected for $CaCO_3$-derived Sr. Notice that the x axis is in log scale.

The observed subsurface pSr maximum suggests a potential prevalence of symbiotic Acantharia in the euphotic zone (**Figure 3b**). Despite *Phaeocystis antarctica*, a primary symbiont of Acantharia in the Southern Ocean (Decelle *et al.*, 2012), dominating the phytoplankton community in the SAZ (Eriksen *et al.*, 2018), the absence of a significant increase in the abundance of *Phaeocystis antarctica* during the phytoplankton blooms (Eriksen *et al.*, 2018),

indicates the pSr flux peaks may not be associated with elevated productivity of symbiotic Acantharia. Additionally, the prevalence of symbiotic Acantharia in the euphotic zone makes them susceptible to dissolution during transport to bathypelagic depths. This further suggests that symbiotic Acantharia may not be the dominant contributor to pSr flux peaks. Recent sequencing data, however, presents the possibility that some symbiotic Acantharia may also reproduce at depth (Mars Brisbin *et al.*, 2020). While symbiotic Acantharia might contribute to POC flux through zooplankton faecal pellets, the acidic microenvironments in zooplankton guts could lead to the dissolution of most Acantharia as this is hypothesized to induce $CaCO_3$ dissolution in $CaCO_3$-saturated seawater (Milliman *et al.*, 1999).

4.7. Potential Drivers of Acantharian Fluxes

The sediment trap deployment across different years demonstrates that Acantharian fluxes vary seasonally, and high fluxes are recurrent each year in January/February in the SAZ. The positive correlation between maximum pSr flux at 1000 m trap and surface chlorophyll *a* concentration (**Figure 5**), as well as the positive correlation between pSr concentration, pP and fluorescence concentrations (**Figure 3**), indicates that the Acantharia sinking flux is indeed linked to phytoplankton productivity, as hypothesized by Martin *et al.* (2010) and Decelle *et al.* (2013). During phytoplankton productive season, Acantharia can rapidly increase their population size by actively feeding on the plankton (Henjes *et al.*, 2007; Jacquet *et al.*, 2007). Subsequently, they form dense cysts to rapidly sink to bathypelagic depths to release swarmers. In addition to productivity, temperature emerges as a crucial driver of elevated Acantharia biomass in summer, given their abundance in tropical and subtropical waters (Decelle and Not, 2015). The pSr export flux peaks simultaneously with the second peak of POC during the period of highest ocean temperature (~12˚C) in this study, highlighting the importance of temperature maxima in initiating Acantharia productivity in high-latitude oceans. The rapid warming in the Southern Ocean (Gille, 2008) due to the southward migration of ACC fronts (Sokolov and Rintoul, 2009) introduces a potential impact on the contribution of Acantharia to POC flux. On the one hand, the warming is expected to stimulate growth rates of all pelagic organisms, including Acantharia, potentially elevating their significance in POC export flux. On the other hand, ocean warming will alter the seasonal extent of areas favourable for deep reproduction (e.g. Sorte, Williams and

Carlton, 2010), potentially leading to shallower sedimentation of Acantharia and a reduced contribution to POC export flux.

5. Conclusions

This study explores the role of Acantharia in Sr and C cycles in the Southern Ocean by examining dissolved and particulate Sr concentrations alongside sediment trap fluxes at 1000 m. The decoupling between surface dSr concentration and pSr flux at 1000 m could be attributed to the different integration time of Sr cycling represented by the two, and limited pSr impact on dSr. Acantharia are the primary driver of dSr, generating a vertical and latitudinal gradient of dSr in the Southern Ocean. Sediment trap data suggests that pSr fluxes are seasonal, with intense pSr flux events reoccurring annually which can be attributed primarily from Acantharia, despite $CaCO_3$ making a major contribution to pSr flux in non-productive season. These high pSr flux events coincide with the secondary peak in POC export during the austral summer, highlighting the association of Acantharia biomass not only with productivity but also with ocean temperature. Despite the modest contribution of Acantharia to annual POC flux at 1000 m and its minimal importance in export flux compared to calcareous plankton, Acantharia can significantly contribute to POC export, particularly during the austral summer phytoplankton bloom development.

Acknowledgments

Thanks to Gemma Woodward and Diana M. Davies for providing the archived SOTS mooring samples analyzed in this study. We thank Elizabeth Shadwick for useful comments on manuscripts. The authors are grateful to the officers, crew, and research staff of the Marine National Facility and the *RV Investigator* for their help with sample collection and generation of hydrochemistry data on voyages IN2018_V01 and IN2020_V08. This research was supported by a grant of sea time on *RV Investigator* from the CSIRO Marine National Facility (https://ror.org/01mae9353). We thank Chief Scientists Steve Rintoul (IN2018_V01) and Philip Boyd (IN2020_V08) for supporting dissolved sample collection for this study. The SOTS observatory is supported by Australia's Integrated Marine Observing System (IMOS). IMOS is operated by a consortium of institutions as an unincorporated joint venture, with the University of Tasmania as the Lead Agent. Financial support also came from The Australian Centre for

Excellence in Antarctic Science, which is a Special Research Initiative funded by the Australian Research Council (SR200100008). The Australian Government Research Training Program Domestic Scholarship and the ANU Supplementary Scholarship funding to Yaojia Sun are also acknowledged.

Open Research

The 2-D model results are listed in Table 2. The CTD hydrographic and biogeochemistry data from both voyages are accessible via the Commonwealth Scientific and Industrial Research Organisation (CSIRO) Trawler Data Repository at https://www.cmar.csiro.au/data/trawler/. Additionally, hydrographic and biogeochemistry data along with particle fluxes derived from Southern Ocean Time Series (SOTS) moorings, can be accessed through the Australian Ocean Data Network (AODN) portal at https://portal.aodn.org.au/search. The dissolved and particulate strontium concentration data and strontium flux data are available at https://docs.google.com/spreadsheets/d/1ZLCgyOGgnwT0XDwyaugUrmDIj7RiAta2/edit?usp=share_link&ouid=101414574852942702611&rtpof=true&sd=true or upon request to the corresponding author (yaojia.sun@anu.edu.au).

References

Assmy, P. *et al.* (2014) 'Response of the protozooplankton assemblage during the European Iron Fertilization Experiment (EIFEX) in the Antarctic circumpolar current', *Journal of Plankton Research*, 36(5), pp. 1175–1189. doi: 10.1093/plankt/fbu068.

Balch, W. M. *et al.* (2011) 'The contribution of coccolithophores to the optical and inorganic carbon budgets during the Southern Ocean Gas Exchange Experiment: New evidence in support of the Great Calcite Belt hypothesis', *Journal of Geophysical Research: Oceans*. doi: 10.1029/2011JC006941.

Balch, W. M. *et al.* (2016) 'Factors regulating the Great Calcite Belt in the Southern Ocean and its biogeochemical significance', *Global Biogeochemical Cycles*. doi: 10.1002/2016GB005414.

Belcher, A. *et al.* (2018) 'Acantharian cysts: high flux occurrence in the bathypelagic zone of the Scotia Sea, Southern Ocean', *Marine Biology*. Springer Berlin Heidelberg, 165(7), pp. 1–11. doi: 10.1007/s00227-018-3376-1.

Bernstein, R. E. *et al.* (1987) 'Acantharian fluxes and strontium to chlorinity ratios in the North Pacific Ocean', *Science*, 237(4821), pp. 1490–1494. doi: 10.1126/science.237.4821.1490.

Boyd, P. W. *et al.* (2019) 'Multi-faceted particle pumps drive carbon sequestration in the ocean', *Nature*. Springer US, 568(7752), pp. 327–335. doi: 10.1038/s41586-019-1098-2.

Brass, G. W. and Turekian, K. K. (1974) 'Strontium distribution in Geosecs oceanic profiles', 1(1), pp. 303–335.

584 Caron, D. A. *et al.* (1995) 'Primary productivity by symbiont-bearing planktonic sarcodines
585 (Acantharia, Radiolaria, Foraminifera) in surface waters near Bermuda', *Journal of Plankton*
586 *Research*, 17(1), pp. 103–129. doi: 10.1093/plankt/17.1.103.
587 Decelle, J. *et al.* (2012) 'An original mode of symbiosis in open ocean plankton', *Proceedings of*
588 *the National Academy of Sciences of the United States of America*, 109(44), pp. 18000–18005.
589 doi: 10.1073/pnas.1212303109.
590 Decelle, J. *et al.* (2013) 'Diversity, Ecology and Biogeochemistry of Cyst-Forming Acantharia
591 (Radiolaria) in the Oceans', *PLoS ONE*, 8(1). doi: 10.1371/journal.pone.0053598.
592 Decelle, J. and Not, F. (2015) 'Acantharia', in *eLS*, pp. 1–10. doi:
593 10.1002/9780470015902.a0002102.pub2.
594 De Deckker, P. (2004) 'On the celestite-secreting Acantharia and their effect on seawater
595 strontium to calcium ratios', *Hydrobiologia*, 517(1–3), pp. 1–13. doi:
596 10.1023/B:HYDR.0000027333.02017.50.
597 Deppeler, S. L. and Davidson, A. T. (2017) 'Southern Ocean phytoplankton in a changing
598 climate', *Frontiers in Marine Science*, 4(FEB). doi: 10.3389/fmars.2017.00040.
599 Eriksen, R. *et al.* (2018) 'Seasonal succession of phytoplankton community structure from
600 autonomous sampling at the Australian Southern Ocean Time Series (SOTS) observatory',
601 *Marine Ecology Progress Series*, 589, pp. 13–21. doi: 10.3354/meps12420.
602 Fernández Castro, B. *et al.* (2022) 'Subtropical Contribution to Sub-Antarctic Mode Waters',
603 *Geophysical Research Letters*, 49(11). doi: 10.1029/2021GL097560.
604 Gangstø, R. *et al.* (2008) 'Modeling the marine aragonite cycle: changes under rising carbon
605 dioxide and its role in shallow water CaCO3 dissolution', *Biogeosciences*, 5(4), pp. 1057–1072.
606 doi: 10.5194/bg-5-1057-2008.
607 Gille, S. T. (2008) 'Decadal-Scale Temperature Trends in the Southern Hemisphere Ocean',
608 *Journal of Climate*, 21(18), p. 4749. doi: 10.1175/2008JCLI2131.1.
609 Gowing, M. M. and Garrison, D. L. (1992) 'Abundance and feeding ecology of larger
610 protozooplankton in the ice edge zone of the Weddell and Scotia Seas during the austral winter',
611 *Deep Sea Research Part A, Oceanographic Research Papers*, 39(5), pp. 893–919. doi:
612 10.1016/0198-0149(92)90128-G.
613 Henjes, J. *et al.* (2007) 'Response of the larger protozooplankton to an iron-induced
614 phytoplankton bloom in the Polar Frontal Zone of the Southern Ocean (EisenEx)', *Deep-Sea*
615 *Research Part I: Oceanographic Research Papers*, 54(5), pp. 774–791. doi:
616 10.1016/j.dsr.2007.02.005.
617 Honjo, S. *et al.* (2008) 'Particulate organic carbon fluxes to the ocean interior and factors
618 controlling the biological pump: A synthesis of global sediment trap programs since 1983',
619 *Progress in Oceanography*, 76(3), pp. 217–285. doi:
620 https://doi.org/10.1016/j.pocean.2007.11.003.
621 Jacquet, S. H. M. *et al.* (2007) 'Barium cycling along WOCE SR3 line in the Southern Ocean',
622 *Marine Chemistry*. doi: 10.1016/j.marchem.2006.06.007.
623 Johnson, K. S. *et al.* (2017) 'Annual nitrate drawdown observed by SOCCOM profiling floats
624 and the relationship to annual net community production', *Journal of Geophysical Research:*
625 *Oceans*, 122(8), pp. 6668–6683. doi: 10.1002/2017JC012839.
626 Mars Brisbin, M. *et al.* (2020) 'Paired high-throughput, in situ imaging and high-throughput
627 sequencing illuminate acantharian abundance and vertical distribution', *Limnology and*
628 *Oceanography*, 65(12), pp. 2953–2965. doi: 10.1002/lno.11567.
629 Martin, J. H. *et al.* (1987) 'VERTEX: carbon cycling in the northeast Pacific', *Deep Sea*

Research Part A. Oceanographic Research Papers, 34(2), pp. 267–285. doi: https://doi.org/10.1016/0198-0149(87)90086-0.
Martin, P. *et al.* (2010) 'Sedimentation of acantharian cysts in the Iceland Basin: Strontium as a ballast for deep ocean particle flux, and implications for acantharian reproductive strategies', *Limnology and Oceanography*, 55(2), pp. 604–614. doi: 10.4319/lo.2010.55.2.0604.
Michaels, A. F. (1988) 'Vertical distribution and abundance of Acantharia and their symbionts', *Marine Biology*. Springer, 97, pp. 559–569.
Michaels, A. F. (1991) 'Acantharian abundance and symbiont productivity at the VERTEX seasonal station', *Journal of Plankton Research*, 13(2), pp. 399–418. doi: 10.1093/plankt/13.2.399.
Michaels, A. F. *et al.* (1995) 'Planktonic sarcodines (Acantharia, Radiolaria, Foraminifera) in surface waters near Bermuda: abundance, biomass and vertical flux', *Journal of Plankton Research*, 17(1), pp. 131–163. doi: 10.1093/plankt/17.1.103.
Milliman, J. D. *et al.* (1999) 'Biologically mediated dissolution of calcium carbonate above the chemical lysocline?', *Deep-Sea Research Part I: Oceanographic Research Papers*, 46(10), pp. 1653–1669. doi: 10.1016/S0967-0637(99)00034-5.
North, N. A. (1974) 'Pressure dependence ot SrSO4 solubility', *Geochimica et Cosmochimica Acta*, 38(7), pp. 1075–1081. doi: https://doi.org/10.1016/0016-7037(74)90005-2.
Orsi, A. H., Whitworth, T. and Nowlin, W. D. (1995) 'On the meridional extent and fronts of the Antarctic Circumpolar Current', *Deep-Sea Research Part I*, 42(5), pp. 641–673. doi: 10.1016/0967-0637(95)00021-W.
Reardon, E. J. and Armstrong, D. K. (1987) 'Celestite (SrSO4 (s)) solubility in water, seawater and NaCl solution', *Geochimica et Cosmochimica Acta*. Elsevier, 51(1), pp. 63–72.
Schewiakoff, W. (1926) 'Acantharia. Fauna e flora del Golfo di Napoli. 2 vols', *Staz. Zool. Napol., Monografia*, (37), p. 755.
Schlitzer, R. (2023) 'Ocean Data View'. Available at: odv.awi.de.
Siegel, D. A. and Deuser, W. G. (1997) 'Trajectories of sinking particles in the Sargasso Sea: modeling of statistical funnels above deep-ocean sediment traps', *Deep Sea Research Part I: Oceanographic Research Papers*, 44(9), pp. 1519–1541. doi: https://doi.org/10.1016/S0967-0637(97)00028-9.
Sokolov, S. and Rintoul, S. R. (2009) 'Circumpolar structure and distribution of the antarctic circumpolar current fronts: 2. Variability and relationship to sea surface height', *Journal of Geophysical Research: Oceans*. doi: 10.1029/2008JC005248.
Sorte, C. J. B., Williams, S. L. and Carlton, J. T. (2010) 'Marine range shifts and species introductions: comparative spread rates and community impacts', *Global Ecology and Biogeography*, 19(3), pp. 303–316. doi: https://doi.org/10.1111/j.1466-8238.2009.00519.x.
Spindler, M. and Beyer, K. (1990) 'Distribution, abundance and diversity of Antarctic acantharian cysts', *Marine Micropaleontology*, 15(3–4), pp. 209–218. doi: 10.1016/0377-8398(90)90011-A.
Steiner, Z. *et al.* (2020) 'Dissolved Strontium, Sr/Ca Ratios, and the Abundance of Acantharia in the Indian and Southern Oceans', *ACS Earth and Space Chemistry*, 4(6), pp. 802–811. doi: 10.1021/acsearthspacechem.9b00281.
Steiner, Z. *et al.* (2021) 'On calcium-to-alkalinity anomalies in the North Pacific, Red Sea, Indian Ocean and Southern Ocean', *Geochimica et Cosmochimica Acta*. Elsevier Ltd, 303, pp. 1–14. doi: 10.1016/j.gca.2021.03.027.
Talley, L. D. (2013) 'Closure of the global overturning circulation through the Indian, Pacific,

and southern oceans', *Oceanography*, 26(1), pp. 80–97. doi: 10.5670/oceanog.2013.07.
Trull, T. W. *et al.* (2001) 'Moored sediment trap measurements of carbon export in the Subantarctic and Polar Frontal Zones of the Southern Ocean, south of Australia', *Journal of Geophysical Research: Oceans*. doi: 10.1029/2000jc000308.
Trull, T. W. *et al.* (2018) 'Distribution of planktonic biogenic carbonate organisms in the Southern Ocean south of Australia: a baseline for ocean acidification impact assessment', *Biogeosciences*, 15(1), pp. 31–49. doi: 10.5194/bg-15-31-2018.
de Villiers, S. (1999) 'Seawater strontium and Sr/Ca variability in the Atlantic and Pacific oceans', *Earth and Planetary Science Letters*, 171(4), pp. 623–634. doi: 10.1016/S0012-821X(99)00174-0.
Whitworth III, T. and Nowlin Jr., W. D. (1987) 'Water masses and currents of the Southern Ocean at the Greenwich Meridian', *Journal of Geophysical Research: Oceans*, 92(C6), pp. 6462–6476. doi: https://doi.org/10.1029/JC092iC06p06462.
Wynn-Edwards, Cathryn A. *et al.* (2020) 'Particle Fluxes at the Australian Southern Ocean Time Series (SOTS) Achieve Organic Carbon Sequestration at Rates Close to the Global Median, Are Dominated by Biogenic Carbonates, and Show No Temporal Trends Over 20-Years', *Frontiers in Earth Science*. doi: 10.3389/feart.2020.00329, 2020a.
Wynn-Edwards, Cathryn Ann *et al.* (2020) *Southern Ocean Time Series (SOTS) Quality Assessment and Control - Sediment Trap Particle Fluxes, Version 1.0, 1997-2018.* doi: 10.26198/5dfad21358a8d, 2020b.